Nonequilibrium fluctuations of lipid membranes by the rotating motor protein F$_1$F$_0$-ATP synthase

Víctor G. Almendro-Vedia[a,b], Paolo Natale[a,b], Michael Mell[a], Stephanie Bonneau[c], Francisco Monroy[a,b], Frederic Joubert[c], and Iván López-Montero[a,b,1]

[a]Departamento Química Física I, Universidad Complutense de Madrid, 28040 Madrid, Spain; [b]Instituto de Investigación Sanitaria Hospital 12 de Octubre (imas12), 28041 Madrid, Spain; and [c]Laboratoire Jean Perrin, CNRS, Université Pierre et Marie Curie, 75005 Paris, France

ATP synthase is a rotating membrane protein that synthesizes ATP through proton-pumping activity across the membrane. To unveil the mechanical impact of this molecular active pump on the bending properties of its lipid environment, we have functionally reconstituted the ATP synthase in giant unilamellar vesicles and tracked the membrane fluctuations by means of flickering spectroscopy. We find that ATP synthase rotates at a frequency of about 20 Hz, promoting large nonequilibrium deformations at discrete hot spots in lipid vesicles and thus inducing an overall membrane softening. The enhanced nonequilibrium fluctuations are compatible with an accumulation of active proteins at highly curved membrane sites through a curvature–protein coupling mechanism that supports the emergence of collective effects of rotating ATP synthases in lipid membranes.

giant vesicles | active membranes | mechanical properties | flickering spectroscopy | biological nanorotors

The rotating F$_1$F$_0$-ATP synthase (F$_1$F$_0$-ATPase) is the transmembrane protein complex responsible for the cellular ATP production, a nonspontaneous chemical reaction that is catalyzed in the presence of an electrochemical proton gradient across the lipid membrane (1). The electrochemical gradient or proton-motive force is composed of an electric charge gradient ($\Delta\Psi$) and a chemical proton gradient (ΔpH), which regulate the optimal functionality of the F$_1$F$_0$-ATPase. This mechanism for ATP biosynthesis is functionally and structurally conserved in all kingdoms of life (2). In recent decades, ATP synthesis function has been artificially reconstituted using several model systems. An important achievement was the combined reconstitution of the chloroplast F$_1$F$_0$-ATPase together with a light-inducible proton pump (3). ATP synthesis has been also reconstituted in vitro on different support substrates such as silica particles (4), polymersomes (5), electrode surfaces (6, 7) and nanowires (8), which are potentially exploitable in technological applications. Recently, the *Escherichia coli bo*3 proton transporter and the *E. coli* F$_1$F$_0$-ATPase have been functionally reconstituted into giant unilamellar vesicles (GUVs) by using oppositely charged liposome fusion techniques (9).

GUVs are suitable model membranes that allow the performance of cytomimetic studies using microscopy-assisted methods, where micropipette manipulation techniques (10) and flickering spectroscopy analysis (11, 12) extract the mechanical properties of membranes. In particular, fast video microscopy makes membrane dynamics easily accessible from the stochastic analysis of the membrane fluctuations (12). The GUV model has been exploited in recent years to get quantitative descriptions of the mechanical impact of different transmembrane proteins or supramolecular assemblies on lipid bilayers (13–16). However, the mechanical influence of the rotating F$_1$F$_0$-ATPase on its embedding lipid membrane has not been explored yet. This important issue is of particular interest, as a curvature-inducing mechanism has been suggested for this protein complex in the formation of membrane invaginations (*cristae*) in the inner mitochondrial membrane (17–19).

Here, we report the functional reconstitution of *E. coli* F$_1$F$_0$-ATPase into GUVs composed of a native *E. coli* lipid extract (F$_1$F$_0$-GUVs). By using flickering spectroscopy, we show that F$_1$F$_0$-ATPase activity induces nonequilibrium membrane fluctuations additional to thermal motions at discrete regions of the membrane. Thus, the rotating F$_1$F$_0$-ATPase promoted an overall membrane softening that is detected as a significant decrease of the effective bending modulus and a lowering of surface tension (15). Furthermore, we found an additional relaxation process characterized with a constant rate of $\Gamma_{act} = 20$ s^{-1}, which is found independent of the spatial scale probed. This active relaxation rate coincides with the rotational dynamics of the ATPase enzyme. The nonequilibrium character of the membrane fluctuations accounts for active membrane motions arising from the coupling between the pumping activity of clustered proteins and the bending modes of the membrane.

Materials and Methods

Electroformation of GUVs. Giant vesicles were prepared using the standard electroformation protocol using indium-tin-oxide (ITO)-covered slides (20). GUVs made of *E. coli* total lipid extract (TLE) (*Ec*GUVs) were prepared by transferring on each ITO slide two 5-μL drops of 20 mg/mL *E. coli* TLE. Electroformed F$_1$F$_0$-GUVs (E-F$_1$F$_0$-GUVs) were prepared by spreading on each ITO slide 10 μL of F$_1$F$_0$ small unilamellar vesicles (F$_1$F$_0$-SUVs) (see *Supporting Information* for details). Then, the films were rehydrated in sucrose solution (200 mM, pH 6), and the electrodes were connected to an AC power supply

(500 Hz, 1.1 V; Agilent) for at least 3 h. E-F$_1$F$_0$-GUVs were almost spherical and unilamellar. The size and unilamellarity distributions are shown in Fig. S1.

Detergent-Based Reconstitution of the F$_1$F$_0$-ATPase in GUVs. EcGUVs were prepared by electroformation in the presence of 200 mM sucrose, 0.2 mM of n-Dodecyl-β-d-maltoside (DDM), and 150 μM pH-sensitive fluorescent probe pyranine. Then, F$_1$F$_0$-GUVs produced by detergent removal (D-F$_1$F$_0$-GUVs) were formed by incubating 10 nM purified F$_1$F$_0$-ATPase with 0.25 mg/mL EcGUVs for 2 h at 4 °C. The excess of detergent was removed with SM2 Bio-Beads (Biorad) according to manufacturer's instructions (21).

Activation of F$_1$F$_0$-ATPase On Addition of Valinomycin. Twenty-five microliters of F$_1$F$_0$-GUVs were diluted three times in an iso-osmolar reaction buffer (50 mM KCl, 10 mM K$_2$HPO$_4$, 10 mM Na$_2$ADP, 5 mM MgCl$_2$, and 30 mM Hepes pH 7.2) and incubated for 15 min at 20 °C to let pH equilibrate. F$_1$F$_0$-GUVs were activated on addition of 10 μM valinomycin in ethanol (≤1% vol final concentration) (22). For control experiments, F$_1$F$_0$-GUVs were incubated with the triggering solvent in the absence of valinomycin.

Fluctuation Spectroscopy and Membrane Mechanics. To obtain the spectrum of the membrane fluctuation modes $P(q)$, movies of the fluctuating GUVs are recorded at their equatorial plane by high-velocity video microscopy in the phase contrast mode (see *Supporting Information* for details). At a given time t, the shape fluctuations are described as discrete Fourier modes, that is, $h(t) = \sum_q h_q(t) e^{iqx}$, where $q = l/R_0$ is the equatorial projection of the fluctuation wave vector ($l = 2, 3, 4, \ldots \infty$). The spectrum is given by the variance of the mode amplitudes, which is $P(q) = \mathcal{L}^2 \langle h_q^2 \rangle$ ($\mathcal{L}^2$ is the area of the membrane); for thermal fluctuations (11),

$$P_{th}^{(pass)}(q) = \frac{k_B T}{2\sigma}\left[\frac{1}{q} - \sqrt{\frac{\kappa}{\sigma + \kappa q^2}}\right], \qquad [1]$$

where $k_B T$ is the thermal energy, the bending modulus (κ) and the surface tension (σ) can be obtained by fitting to the experimental mode amplitudes. The case of nonequilibrium modes driven by protein activity has been studied by Prost and coworkers (13, 23, 24). For the equatorial spectrum, they deduced (24)

$$P_q^{(exp)}(q_x) = P_q^{(pass)}(\sigma_{eff}, \kappa_{eff}) + \frac{A k_B T}{4\kappa_{eff}^2\left(q^2 + \frac{\sigma_{eff}}{\kappa_{eff}}\right)^{3/2}}, \qquad [2]$$

with effective mechanical parameters depending on the activity of the protein, and

$$A = \left(F_0^2 - \Xi F_0\right)/4\zeta \qquad [3]$$

being an effective amplitude for the active term. Here, F_0 is a generalized force stressed by the active components, and Ξ is a coupling constant that accounts for the energy involved in creating local curvature by a net imbalance of pumping activity between the two sides of the membrane. The susceptibility involved in creating such imbalance is denoted by ζ (see *Supporting Information* for details). Within the active vesicle theory, this curvature–protein coupling induces a softening that is described as a decrease of the effective bending modulus as (13)

$$\kappa_{eff} = \kappa - \Xi^2/\zeta. \qquad [4]$$

Membrane dynamics can be studied by probing the experimental autocorrelation function (24)

$$\langle h_q(t'-t)h_q(t')\rangle = \langle h_q^2\rangle_{pass} e^{-\Gamma_0 t} + \langle h_q^2\rangle_{act} e^{-\Gamma_{act} t}, \qquad [5]$$

which consists of the ordinary time relaxation of the thermal mechanical mode (passive), plus an extraordinary term that describes correlations within the nonequilibrium (active) fluctuations. For a passive membrane fluctuating in a fluid of viscosity η, the autocorrelation function (ACF) is found as a single-exponential decay for thermal modes with a relaxation rate (25),

$$\Gamma_0 = \left(\sigma q + \kappa q^3\right)/4\eta. \qquad [6]$$

Results

Reconstitution of the E. coli F$_1$F$_0$-ATPase in GUVs. F$_1$F$_0$-GUVs were formed either by electroformation of F$_1$F$_0$-SUVs (26) or by detergent-mediated (27) incorporation of the purified F$_1$F$_0$ complex into preformed EcGUVs (Fig. S2 A and B; see *Materials and Methods* for details). For both types of GUVs, the incorporation

of the F$_1$F$_0$-ATPase was confirmed by Western blotting using specific antibodies that specifically recognize the beta (∼50 kDa) and b subunit (∼17 kDa) of F$_1$ and F$_0$, respectively (Fig. S3). Additionally, we checked the reconstitution of the F$_1$F$_0$ complex into the detergent-mediated GUVs with Alexa-647 labeled F$_1$F$_0$-ATPase. Confocal microscope images show the fluorescence signal of proteins in the GUV membrane (Fig. S2C). After quantification, we found two protein density ranges: $n_0 = 10^{13}$ proteins per square meter (corresponding to an area fraction of 0.15%) for D-F$_1$F$_0$-GUVs and $n_0 = 10^{14}$ proteins per square meter (corresponding to an area fraction of 1.5%) for E-F$_1$F$_0$-GUVs.

Then we checked the enzymatic activity of F$_1$F$_0$-ATPase in GUVs (Fig. 1A). ATP synthesis is triggered by the addition of the selective K$^+$ transporter valinomycin (22). As a consequence of K$^+$ internalization, protons are pumped out through the rotating proton channel of the F$_0$ subunit. The presence of the pH-sensitive fluorescent probe pyranine is used as a reporter to visualize luminal basification (28), which is indicative for ATP synthesis, as both enzymatic processes are strictly correlated. After valinomycin addition, we observed an average increase of fluorescence in the lumen of F$_1$F$_0$-GUVs (Fig. 1B, *Top*). The green luminal fluorescence increased until it reached a plateau after several minutes of incubation. In contrast, we did not observe any pyranine fluorescence intensity increase in EcGUVs experiments performed in the absence of F$_1$F$_0$ proteins (Fig. 1B, *Bottom*). The average increase of fluorescence corresponded to a ΔpH of 1.5 to 2 units (Fig. S4) as measured from the calibration curves shown in Fig. S5 (see *Supporting Information* for details). The distribution of the basification rates is shown in Fig. S6. Both E-F$_1$F$_0$-GUVs and D-F$_1$F$_0$-GUVs displayed similar distributions, as a vast majority of vesicles had a basicity rate of $k_b \approx 0.01$ min^{-1}. This indicates that both F$_1$F$_0$-GUVs presented similar protein activity. Despite a more efficient reconstitution of the F$_1$F$_0$ complex in E-F$_1$F$_0$-GUVs, the electroformation process in the absence of salts may be harmful for proteins, and the effective concentration of proteins could be reduced. Even so, a small fraction of E-F$_1$F$_0$-GUVs showed larger basicity rates in comparison with D-F$_1$F$_0$-GUVs, in agreement with a higher protein/lipid ratio on reconstitution.

Although the lumen increase of pH adjusts to the expected ΔpH as calculated by the Nernst potential due to K$^+$ internalization, an independent measurement of the membrane potential by the fluorescent probe Rhodamine 123 indicates that the reconstituted F$_1$F$_0$ complexes are not able to completely compensate the membrane potential triggered by the valinomycin molecules (Fig. S7). After the initial regime of rapid ATP synthesis rate, the protein activity is expected to be maintained, as ΔΨ is not completely dissipated and the ATP synthesis by F$_1$F$_0$-ATPase of *E. coli* depends on the presence of an electric membrane potential (29).
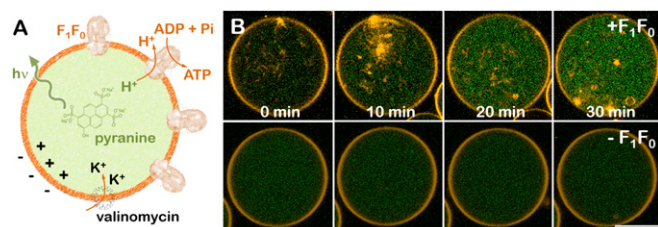
Fig. 1. Reconstitution of the *E. coli* F$_1$F$_0$-ATPase in GUVs. (A) Schematic cartoon of F$_1$F$_0$-ATPase reconstitution into giant vesicles (*Left*). ATP synthesis is triggered on valinomycin incubation that creates a membrane potential, positive in the lumen of the vesicle. Proton outward translocation through F$_1$F$_0$-ATPases is monitored by the pH-sensitive fluorophore pyranine (green). The lipid bilayer was doped with 0.5% mol RhPE (orange dye). (B) Proton efflux kinetics of *E. coli* GUVs on valinomycin incubation as observed under fluorescence microcopy, in the presence (*Top*) and in the absence (*Bottom*) of F$_1$F$_0$-ATPases. (Scale bar: 10 microns.)
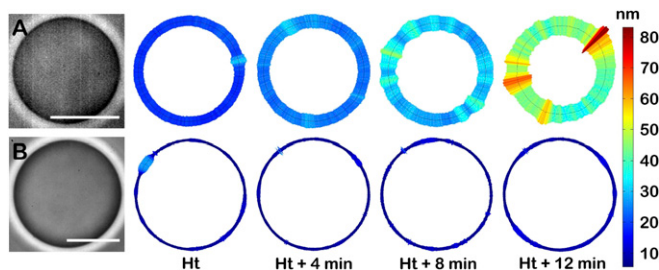
Fig. 2. Membrane fluctuations of single D-F_1F_0-GUVs. Typical membrane fluctuation maps of a single D-F_1F_0-GUV at different time intervals (Ht, handling time) under (*A*) active conditions and (*B*) passive conditions. Scale bar represents the SD value (RMSD in nanometers) of the local membrane fluctuations measured in real space at the equatorial vesicle plane as $h(i,t) - h_0$, where h accounts for the time membrane position i and h_0 is the time average value. For illustration, see Movie S1.

Membrane Fluctuations. To directly observe the impact of the ATP synthesis on the bending properties of lipid membranes, we performed single-vesicle fluctuation spectroscopy on F_1F_0-GUVs under ATP-producing (active) and non-ATP-producing (passive) conditions (Movie S1). Fig. 2 illustrates the membrane fluctuation maps of single GUVs, which are obtained as the root mean SD (RMSD = $\sigma_h = \langle h^2 \rangle^{1/2}$) of the local fluctuation time traces recorded at different time intervals counted from the beginning of the reaction. On the addition of valinomycin, F_1F_0-GUVs membrane fluctuations became larger during protein activity and were characterized as membrane displacements far away from the equilibrium position (Fig. 2*A*). This observation correlates with the increasing protein activity established by the increasing $\Delta\Psi$ during the first 20 min after the addition of valinomycin (Fig. S7). Moreover, active F_1F_0-GUVs showed enhanced fluctuations at discrete regions of the membrane, whose relative position varied from one time interval to another. The passive F_1F_0-GUVs exhibited initially similar but low fluctuations than active F_1F_0-GUVs (Fig. 2*B*). In this case, the fluctuations remained weak in amplitude along time and were characterized by a low value of the SD ($\sigma_h^{(pass)} \approx 15$ nm). Nonetheless, the active vesicles displayed increasing enhanced fluctuations when tracked for the same time intervals as in the passive case ($\sigma_h^{(act)}(t) \geq \sigma_h^{(pass)}$). Unlike passive vesicles, which remained fluctuating for longer times, active vesicles lose optical contrast and become unstable.

The statistical characterization of the membrane fluctuations was performed using the ensemble-averaged probability density function (PDF) (*Supporting Information*), which was calculated over all of the points in the contour profile and over a statistically significant population of single vesicles ($n \geq 20$). For passive F_1F_0-GUVs, the ensemble-averaged PDF is found to be nearly Gaussian (with a narrow and nearly symmetric quadratic signature in the logarithmic plot, Fig. S8*A*) as expected for thermal fluctuations. The membrane fluctuations were characterized by an RMSD value, $\sigma_0 = 16.3 \pm 0.3$ nm, which remains unchanged over time. However, active F_1F_0-GUVs exhibited enhanced fluctuations, and the PDFs were found to progressively broaden over time (Fig. S8*B*). In this case, we found that the SD values shifted to higher values with increasing times: $\sigma_{Ht+4} = 25.6 \pm 0.1$ nm, $\sigma_{Ht+8} = 32.1 \pm 0.3$ nm, and $\sigma_{Ht+12} = 32.7 \pm 0.3$ nm. Regarding the higher PDF moments, they remained essentially compatible with the Gaussian characteristics in both cases (the third moment, or skewness, $S = 0$, and the fourth one, or kurtosis, $K = 3$; Fig. S8, *Insets*).

Further, we explored the presence of locally non-Gaussian distributions (Fig. 3) at the specific membrane sites with magnified levels of membrane fluctuations, or hot spots (Fig. 2*A*). For the passive case, F_1F_0-GUVs were systematically characterized by almost normal Gaussian distributions along the membrane contour (Fig. 3 *A* and *B*), in agreement with the

intrinsically symmetric nature of the thermal fluctuations. However, under active conditions, a non-Gaussian distribution of the membrane displacements is observed for different hot spots, which are generally right-skewed ($S > 0$) and leptokurtic ($K > 3$), as revealed by the longer tails than expected for the normal distribution (Fig. 3 *C* and *D*, respectively). The positive skew is compatible with a vectorized protein pumping toward the outer side of the membrane. As a representative example of this asymmetric behavior, we zoom on the mechanical hot spot 1 ($S = 1.2$, and $K = 5.8$) and hot spot 3 ($S = 0.5$, and $K = 4$), whereas the fluctuations in the low-activity sites (spots 2 and 4) distribute almost Gaussian ($S \approx 0$; $K \approx 3$). Because the majority of the membrane contour points display a Gaussian behavior, they mask the non-Gaussian signature of the hot spots when ensemble-averaged by the rest of the thermalized contour membrane points (Fig. S8*B*). Note that, according to the measured n_0, the protein area fraction is 0.15 to 1.5%, so that the number of active hot spots per contour GUV should be 3 to 30, in agreement with our observations.

Membrane Mechanical Properties. The experimental fluctuation spectra were obtained at different time intervals for both active and passive cases (Fig. 4*A*). Regarding q scaling, an evident difference is observed between passive and active cases. Helfrich-like scaling is observed for the passive vesicles (Fig. 4*A*, *Top Right*), which is characterized by a regular crossover between tension-dominated ($P \approx q^{-1}$ at low q) down to a bending regime ($P \approx q^{-3}$ at high q) (Eq. 1). However, the spectral amplitudes of the active vesicles are characterized by a low-q pseudoplateau ($P \approx q^0$), which is characteristic of the tension-dominated regime of the active spectrum (see Eq. 2 for $A > 0$ at $\sigma_{eff} \gg \kappa_{eff} q^2$). A decrease in the bending energy is pointed out as a progressive increase of the fluctuation amplitudes at low wave vectors, where the fluctuation modes are mainly driven by an active force
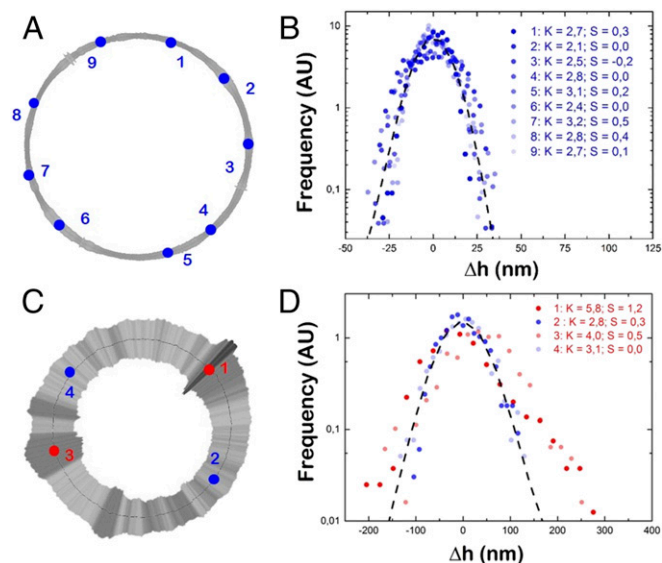
Fig. 3. Mechanical hot-spots of D-F_1F_0-GUVs. (*A*) Fluctuation map of passive D-F_1F_0-GUV from *B* (t = Ht + 12 min). Points indicate the membrane positions where the PDF is calculated in *B*. (*B*) PDF at different points highlighted in *A*. Dashed line represents the ensemble-averaged PDF as calculated for all contour points of the vesicle. (*C*) Active D-F_1F_0-GUV from *A* (t = Ht + 12 min). Points indicate membrane positions where the PDF is calculated in *D*. (*D*) PDF at different points highlighted in *C*. Dashed line represents the ensemble-averaged PDF as calculated for all points of the vesicle. PDFs from points 1 and 3 deviate from Gaussianity. Note that *B* and *D* have different scales to highlight the probable out-of-equilibrium signature of hot spots.
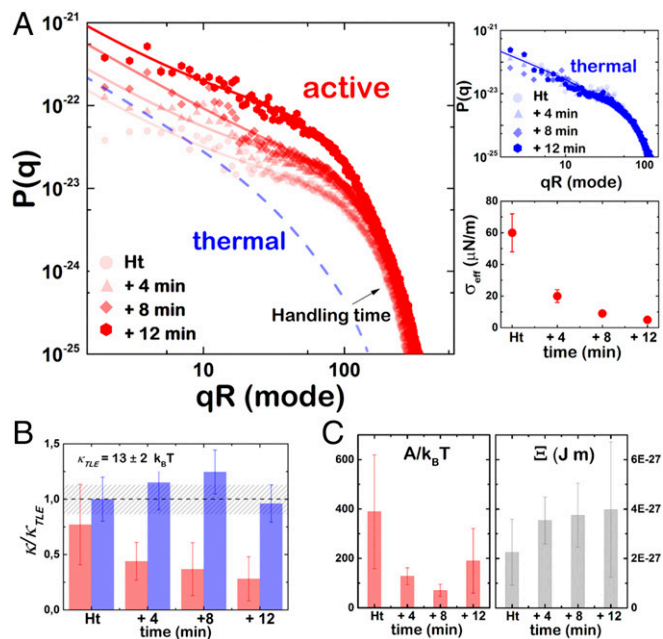
Fig. 4. Fluctuation spectrum and mechanical properties. (*A*) Experimental fluctuation spectra obtained for a typical active D-F_1F_0-GUV at different time intervals after valinomycin incubation. Solid lines represent the best fit to Eq. **2**. The dashed line represents the fit to Eq. **1** for the passive case ($t = $ Ht) as shown in *Top Right*. (*Top Right*) Experimental fluctuation spectra obtained for a typical passive D-F_1F_0-GUV at different time intervals. Solid lines represent the best fit to Eq. **1**. (*Bottom Right*) Variation of the effective surface tension σ at different time intervals after valinomycin incubation. (*B*) Variation of the population-averaged bending rigidity, κ, of active (red, $n = 23$) and passive (blue, $n = 33$) D-F_1F_0-GUVs measured at different time intervals. Bending rigidity is normalized to the bending rigidity measured for pure lipid EcGUVs, κ_{TLE}. The dashed region represents the dispersity on the lipid bending modulus, κ_{TLE}. (*C*) (*Left*) Variation of the effective activity, A, of active ($n = 23$) D-F_1F_0-GUVs at different time intervals. (*Right*) Variation of the coupling parameter (Ξ) at different time intervals after valinomycin incubation.

exceeding the thermal energy and mainly restored by surface tension (Fig. 4*A*, *Left*). By contrast, only the thermal contribution is observed in this region of the fluctuation spectra under non-active conditions (Fig. 4*A*, *Top Right*).

The effective values of the mechanical parameters can be obtained by fitting the experimental equatorial spectra to Eqs. **1** and **2**. The progressive membrane softening observed under ATP synthesis was quantified as a decrease of the effective bending modulus due to protein activity (Eq. **4**). The elastic parameters for active and passive F_1F_0-GUVs and EcGUVs are shown in Fig. 4*B*. EcGUVs represented the basal level of membrane fluctuation that corresponds to the rigidity of the bare lipid membrane with a statistically averaged bending modulus of $\kappa_{lipid} = (13 \pm 2) \, k_BT$. The incorporation of proteins at low density (up to 1.5% in our case) into lipid membranes is not expected to produce significant compositional impact on the membrane rigidities (30); thus the measured value of bending stiffness in F_1F_0-GUVs was similar to that in EcGUVs and remained unchanged over time (Fig. 4*B*). Remarkably, on F_1F_0 activation, the value of bending rigidity significantly decreased by a quarter of the initial value compatible with the passive case. This mechanical softening can be understood as a dynamical effect that connects the F_1F_0 activity with the overall membrane softening. With respect to surface tension, no significant changes of the averaged population values were detected during protein activity. The high variability of this mechanical parameter among different vesicle specimens is due to the broadly variable excess area that is created in every single vesicle using electroformation (25) (see *Supporting Information* for a detailed

explanation). However, a systematic decrease of the effective value is observed for individual specimens undergoing nonequilibrium fluctuations (Fig. 4*A*, *Bottom Right*), in agreement with similar active systems with protein pumps (15, 31).

The quantitative spectral analysis in terms of active vesicle theory allows for a discrimination of a nonequilibrium fluctuation regime. Particularly, the amplitude of the active component A was evaluated (Fig. 4*C*, *Left*). On average, we measured initial values of $A \approx 400 \, k_BT$ that decreased over time to values close to $150 \, k_BT$. The global decrease observed in the active term, which is concomitant with a monotonical decrease in the bending modulus, reflects the nontrivial dependence of the effective amplitude A on activity. In effect, A is proportional to the force, F_0, exerted by the active proteins according to Eq. **3**, but also decreases with the strength of the coupling term Ξ, which might depend itself on the pumping activity. From Eq. **4**, higher values of Ξ are obtained under continuous fluctuation enhancement (Fig. 4*C*, *Right*). Thus, the observed decrease of A over time indicates the progressive dominance of the coupling term, whereas F_0 remains essentially constant. From the fits, the value of F_0 can be deduced, which is of the order of $F_0 = 10^{-25}$ to 10^{-26} J m (taking our experimental value for $n_0 = 10^{13} \, m^{-2}$ and $10^{14} \, m^{-2}$, respectively). This estimation for F_1F_0-ATPase seems higher than previous values obtained from micropipette and shape fluctuation experiments with GUVs containing the pumping membrane protein bacteriorhodopsin (13, 31). However, once the protein densities are considered, similar values of A are obtained for the two proteins. This energy can be related to the energy barrier that the pumping proteins must overcome during the proton transfer process. Whereas this barrier is of the order of 10 kcal/mol for bacteriorhodopsin (32), the torque required for a full rotation of the ATPase motor corresponds to a free energy barrier of 14 kcal/mol, which is supplied by the proton gradient (*Discussion*). Finally, note that the increasing of the coupling constant Ξ can be interpreted in terms of localized protein activity, which may eventually reach the onset of instability predicted in ref. 24, a fact compatible with the presence of localized nonequilibrium fluctuations at the hot spots where the protein could be clustered.

Time Correlation Function and Relaxation Dynamics. Additional evidence on the nonequilibrium character of the membrane fluctuations during ATP synthesis arises from the analysis of the relaxation dynamics of the membrane fluctuations that are obtained from the height-to-height time ACF (*Materials and Methods*). Fig. 5 *A* and *B* shows typical experimental ACFs calculated for the first equatorial fluctuation modes for passive and active F_1F_0-GUVs, respectively. In Fig. 5*C*, we show the relaxation rates obtained from the single-exponential fittings for the passive case (Eq. **5** for $\langle h_q^2 \rangle_{act} = 0$, when $A = 0$). The mechanical parameters were obtained by fitting the experimental relaxation rates to Eq. **6** (see *Supporting Information* for details). We obtained $\kappa_{pass} = 14 \pm 3 \, k_BT$ ($n = 10$ vesicles), in agreement with the values previously obtained from the time-averaged fluctuation spectra (Fig. 4). However, ACFs from active F_1F_0-GUVs exhibited the two-exponential decay predicted by Eq. **5** from active vesicle theory (Fig. 5*B*), which describes two relaxation modes. As in passive F_1F_0-GUVs, the relaxation rate of the faster mode showed the same power-law dependence as described by the thermal mode (Fig. 5*D*). Note that, in the active theory, both the surface tension and the bending modulus contain the active contribution to the relaxation rates (13). From our experiments, an effective value of the bending rigidity $\kappa_{eff} = 2 \pm 1 \, k_BT < \kappa_{pass}$ is obtained ($n = 7$ vesicles), whereas a systematic decrease of the effective value of surface tension is detected in every single vesicle after protein activation. This result is in quantitative agreement with the effective decrease in the bending modulus and the tension lowering observed from the fluctuation spectra in active F_1F_0-GUVs, as shown in Fig. 4. Furthermore, whereas the thermal mode is found to be dispersive, the second relaxation mode

Almendro-Vedia et al.
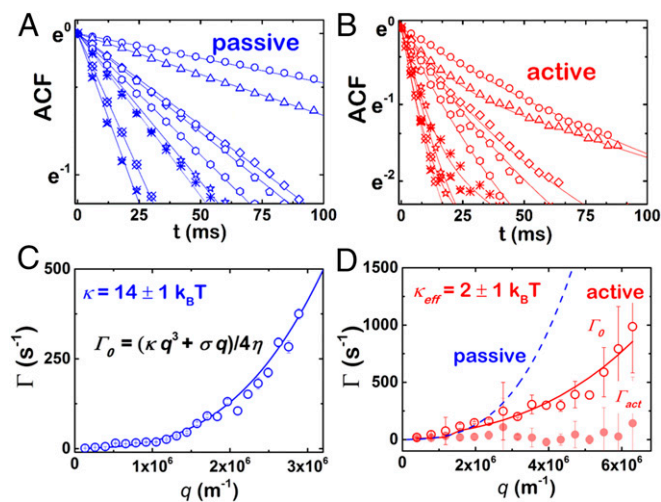
Fig. 5. Time correlation function and relaxation dynamics. Experimental ACFs of a D-F_1F_0-GUV in the (*A*) passive and (*B*) active cases for azimuthal wave vectors $2 \leq l \leq 10$. Solid lines correspond to fits of the experimental data to Eq. **5**. Only the thermal contribution of Eq. **5** was necessary under passive conditions, whereas the bimodal function of Eq. **5** was required for active D-F_1F_0-GUVs. Relaxation rates of a D-F_1F_0-GUV in the (*C*) passive and (*D*) active cases. Thermal frequencies, Γ_0, were fitted using Eq. **S8** with $\eta = 1$ cP (solid lines). For comparison, dashed line in *D* corresponds to the thermal rate shown in *C*. Γ_{act} is the characteristic rate of the metabolic active mode.

appears always with a nearly *q*-independent relaxation rate, which suggests a metabolic origin that could be related to the characteristic rate of the enzymatic activity of the protein (15). The relaxation dynamics of active F_1F_0-GUVs was characterized by a constant rate, at $\Gamma_{act} = 20 \pm 5$ s^{-1}.

As a main outcome of our results, we have demonstrated the functional reconstitution of F_1F_0-ATPase in GUVs, and evidenced that the ATP synthesis activity of the F_1F_0-ATPase promotes enhanced nonequilibrium membrane fluctuations that modify the mechanical properties of the embedding lipid bilayer.

Discussion

According to the conventional Helfrich theory (33, 34), the amplitudes of the thermal fluctuations become progressively smaller at higher wave vectors. Thus, bending-mediated fluctuations prevent large-amplitude deformations at the nanoscale if excited by passive thermal agitation alone. However, cell membranes exhibit a plethora of morphologies in the nanometric scale, including highly curved membranes of some organelles, such as the Golgi, the endoplasmic reticulum, and the inner mitochondrial membrane. Cells take advantage of membrane-associated proteins to promote and stabilize these local membrane deformations either by scaffolding (35, 36) or by wedging (37, 38) mechanisms.

Bending-effector proteins stress membrane distortion that affects the mechanical behavior of the hosting bilayer. Protein activity can contribute to decrease the bending energy of lipid bilayers, as already detected in giant vesicles containing bacteriorhodopsin (13, 31), Ca^{2+} ATPase (14), Na^+ ATPase (15), or K^+ ATPase (37). Our observational results with active vesicles containing F_1F_0-ATPase reveal enhanced fluctuations at localized hot spots in the vesicle membrane that translate into a global lowering in surface tension, which is predominant over long distances, and a decrease in the bending modulus of the membrane at high wave vectors. As F_1F_0-ATPase is not only a proton pump but also a rotating motor through the membrane-spanning component, F_0, two possible effecting modes can be attributed to F_1F_0-ATPase to explain the enhanced membrane fluctuations: a transverse mode connected with the

proton-pumping activity of the enzyme, and an in-plane rotating mode connected to the directional torque of the protein rotor.

Pumping. The coupling mechanism existing between transverse flow of protons across the membrane and the lateral stresses explains the observed lowering in surface tension, as shown for the case of the proton-pumping activity of bacteriorhodopsin (31). Likewise, the coupling between the protein density and the bending elasticity of the membrane can be invoked to explain the observed membrane softening (24). Indeed the nonequilibrium fluctuations found at hot spots are compatible with a pumping-driven undulation of the membrane due to the action of clustered proteins (24). In structural terms, the ability of conic-like ATP synthase dimers to partition into highly curved membranes has been also proposed to induce membrane curved shapes characterized by a wedge angle within the range of 55° and 120° (18, 19). This wedged configuration gives structural support to a positive spontaneous curvature ($C_0 > 0$) and thus to a localized membrane softening [$\kappa_{eff} = \kappa (1 - C_0 R)^2 < \kappa$] (39). Furthermore, above a given concentration threshold for protein clustering, the dynamic coupling between protein and curvature can elicit a membrane instability through localized high-amplitude fluctuations (24), as observed at long times in our experimental realization.

Rotation. The pumping-driven clustering of F_1F_0-ATPases might possibly involve a facilitated protein diffusion of rotating motors through a long-range hydrodynamic interaction mediated by the viscoelastic substrate (40). Indeed, active rotation in a dense medium gives rise to effective interactions between rotors that promote clustering, phase separation, spatial ordering, and synchronization (41–45). These effects remain experimentally unexplored in the case of F_1F_0-ATPase, but the localized nonequilibrium membrane fluctuations we report here can be explained as a consequence of the collective behavior of simultaneous pumping protein clusters mediated by molecular rotation. To identify the characteristic rotation time for an individual rotor, the generated torque by F_0-ring rotation can be estimated as $\mathbf{T} = \boldsymbol{\xi} \times \boldsymbol{\omega} = 6\pi\mu R^2 \ \omega$; where ξ is the drag force of a disk embedded in 2D medium, ω is the angular velocity, μ is the surface membrane viscosity, and R is the radius of the F_0 ring. Taking previously reported values for $\mu = 10^{-5}$ N·s·m^{-1} (46), $R = 5$ nm (47), and the experimentally measured characteristic rate $\omega = \Gamma_{act} = 20 \pm 5$ s^{-1}, we obtain a frictional torque of about 100 ± 25 pN nm. This value is similar to that reported previously for *E. coli* F_1F_0-ATPase (6, 48, 49) and corresponds to the metabolic energy put into play in a rotating cycle of the F_1F_0-ATPase to hydrolyze/synthetize three molecules of ATP. The agreement of these estimations with biochemical information suggests that the time correlation of the active component actually corresponds to the rotational movements of the F_0 ring during ATP synthesis. Therefore, we identify dynamical correlations at a mesoscopic scale, which may correspond to the F_0-ring rotation time in lipid membranes and in the absence of any probe that may eventually drag its rotatory motion.

Furthermore, the correlation decay time of the active component, Γ_{act}, might be predicted from an alternative bending energy formulation. The rotational movements of the F_0 ring during ATP synthesis could be transmitted to the lipid membrane environment by a torsional–curvature coupling mechanism, as lipid reorganization can take place at the vicinity of rotating proteins (50). In a simple dynamical modeling, a metabolic rotator is coupled with the bending mode of the membrane, causing an additional susceptibility, $\chi_{act} \approx (T/V_0)\nabla^2 h$, where T is the torque power stroke of the rotor and V_0 is the molecular volume where rotation takes place. Thus, whereas the thermal mode relaxation depends on the bulk viscosity, the active mode due to metabolic activity of the rotator might relax through the shear viscosity of the embedding membrane, with the hydrodynamic compliance $\Lambda_{memb} = 4\mu q^2$

. Consequently, the active mode is expected to relax at a q-independent constant rate $\Gamma_{act} \approx \chi_{act}/\Lambda_{memb} \approx T/(\mu A_0) \approx 10 \text{ s}^{-1}$ in agreement with our experimental observations (here, $A_0 \approx V_0/h$ is the molecular area of the rotor).

In summary, we present experimental evidence that the coupled pumping and rotation activities of F_1F_0-ATPase promote localized nonequilibrium membrane fluctuations where the active proteins might be clustered. The activity of F_1F_0-ATPase favors the decrease in the bending stiffness of the membrane and the concomitant lowering of its surface tension. Our results point out the existence of a functional connection between microscopic protein activity, supramolecular organization, and macroscopic mechanics, which could be not only operating as a protein activity modulator or as an effector of membrane remodeling in vivo but also exploited in synthetic realizations containing F_1F_0-ATPase within viscoelastic media.

1. Mitchell P (1961) Coupling of phosphorylation to electron and hydrogen transfer by a chemi-osmotic type of mechanism. *Nature* 191:144–148.
2. Jonckheere AI, Smeitink JAM, Rodenburg RJT (2012) Mitochondrial ATP synthase: Architecture, function and pathology. *J Inherit Metab Dis* 35:211–225.
3. Steinberg-Yfrach G, et al. (1998) Light-driven production of ATP catalysed by F0F1-ATP synthase in an artificial photosynthetic membrane. *Nature* 392:479–482.
4. Luo T-JM, Soong R, Lan E, Dunn B, Montemagno C (2005) Photo-induced proton gradients and ATP biosynthesis produced by vesicles encapsulated in a silica matrix. *Nat Mater* 4:220–224.
5. Choi H-J, Montemagno CD (2005) Artificial organelle: ATP synthesis from cellular mimetic polymersomes. *Nano Lett* 5:2538–2542.
6. Naumann R, et al. (1997) Coupling of proton translocation through ATPase incorporated into supported lipid bilayers to an electrochemical process. *Bioelectrochem Bioenerg* 42:241–247.
7. Gutiérrez-Sanz Ó, et al. (2016) H2-fueled ATP synthesis on an electrode: Mimicking cellular respiration. *Angew Chem Int Ed Engl* 55:6216–6220.
8. McBee TW, Cornelius F, Ipsen JH, Mouritsen OG (2006) Characterization of proton transport across a waveguide-supported lipid bilayer. *J Am Chem Soc* 128:2184–2185.
9. Biner O, Schick T, Müller Y, von Ballmoos C (2016) Delivery of membrane proteins into small and giant unilamellar vesicles by charge-mediated fusion. *FEBS Lett* 590:2051–2062.
10. Baumgart T, Das S, Webb WW, Jenkins JT (2005) Membrane elasticity in giant vesicles with fluid phase coexistence. *Biophys J* 89:1067–1080.
11. Pécréaux J, Döbereiner HG, Prost J, Joanny JF, Bassereau P (2004) Refined contour analysis of giant unilamellar vesicles. *Eur Phys J E Soft Matter* 13:277–290.
12. Rodríguez-García R, et al. (2009) Bimodal spectrum for the curvature fluctuations of bilayer vesicles: Pure bending plus hybrid curvature-dilation modes. *Phys Rev Lett* 102:128101.
13. Manneville JB, Bassereau P, Ramaswamy S, Prost J (2001) Active membrane fluctuations studied by micropipet aspiration. *Phys Rev E Stat Nonlin Soft Matter Phys* 64:021908.
14. Girard P, Prost J, Bassereau P (2005) Passive or active fluctuations in membranes containing proteins. *Phys Rev Lett* 94:088102.
15. Bouvrais H, Cornelius F, Ipsen JH, Mouritsen OG (2012) Intrinsic reaction-cycle time scale of Na+,K+-ATPase manifests itself in the lipid–protein interactions of nonequilibrium membranes. *Proc Natl Acad Sci USA* 109:18442–18446.
16. López-Montero I, Rodríguez-García R, Monroy F (2012) Artificial spectrin shells reconstituted on giant vesicles. *J Phys Chem Lett* 3:1583–1588.
17. Allen RD (1995) Membrane tubulation and proton pumps. *Protoplasma* 189:1–8.
18. Minauro-Sanmiguel F, Wilkens S, García JJ (2005) Structure of dimeric mitochondrial ATP synthase: Novel F0 bridging features and the structural basis of mitochondrial cristae biogenesis. *Proc Natl Acad Sci USA* 102:12356–12358.
19. Davies KM, Anselmi C, Wittig I, Faraldo-Gómez JD, Kühlbrandt W (2012) Structure of the yeast F1Fo-ATP synthase dimer and its role in shaping the mitochondrial cristae. *Proc Natl Acad Sci USA* 109:13602–13607.
20. Mathivet L, Cribier S, Devaux PF (1996) Shape change and physical properties of giant phospholipid vesicles prepared in the presence of an AC electric field. *Biophys J* 70:1112–1121.
21. Rigaud JL, Pitard B, Levy D (1995) Reconstitution of membrane proteins into liposomes: Application to energy-transducing membrane proteins. *Biochim Biophys Acta* 1231:223–246.
22. Bhattacharyya P, Epstein W, Silver S (1971) Valinomycin-induced uptake of potassium in membrane vesicles from *Escherichia coli*. *Proc Natl Acad Sci USA* 68:1488–1492.
23. Prost J, Bruinsma R (1996) Shape fluctuations of active membranes. *Europhys Lett* 33:321–326.
24. Ramaswamy S, Toner J, Prost J (2000) Nonequilibrium fluctuations, traveling waves, and instabilities in active membranes. *Phys Rev Lett* 84:3494–3497.
25. Milner ST, Safran SA (1987) Dynamical fluctuations of droplet microemulsions and vesicles. *Phys Rev A Gen Phys* 36:4371–4379.
26. Girard P, et al. (2004) A new method for the reconstitution of membrane proteins into giant unilamellar vesicles. *Biophys J* 87:419–429.
27. Dezi M, Di Cicco A, Bassereau P, Lévy D (2013) Detergent-mediated incorporation of transmembrane proteins in giant unilamellar vesicles with controlled physiological contents. *Proc Natl Acad Sci USA* 110:7276–7281.
28. Seigneuret M, Rigaud JL (1985) Use of the fluorescent pH probe pyranine to detect heterogeneous directions of proton movement in bacteriorhodopsin reconstituted large liposomes. *FEBS Lett* 188:101–106.
29. Kaim G, Dimroth P (1998) ATP synthesis by the F1Fo ATP synthase of *Escherichia coli* is obligatorily dependent on the electric potential. *FEBS Lett* 434:57–60.
30. Hackl W, Seifert U, Sackmann E (1997) Effects of fully and partially solubilized amphiphiles on bilayer bending stiffness and temperature dependence of the effective tension of giant vesicles. *J Phys II* 7:1141–1157.
31. El Alaoui Faris MD, et al. (2009) Membrane tension lowering induced by protein activity. *Phys Rev Lett* 102:038102.
32. Bondar AN, Elstner M, Suhai S, Smith JC, Fischer S (2004) Mechanism of primary proton transfer in bacteriorhodopsin. *Structure* 12:1281–1288.
33. Helfrich W (1973) Elastic properties of lipid bilayers—Theory and possible experiments. *Z Naturforsch C* 28:693–703.
34. Helfrich W, Servuss RM (1984) Undulations, steric interaction and cohesion of fluid membranes. *Nuovo Cimento D* 3:137–151.
35. Rao Y, Haucke V (2011) Membrane shaping by the Bin/amphiphysin/Rvs (BAR) domain protein superfamily. *Cell Mol Life Sci* 68:3983–3993.
36. Sorre B, et al. (2011) How dynamin and amphiphysin sense and generate membrane curvature. *Biophys J* 100(Suppl 1):30a.
37. Aimon S, et al. (2014) Membrane shape modulates transmembrane protein distribution. *Dev Cell* 28:212–218.
38. Devaux PF, Herrmann A, Ohlwein N, Kozlov MM (2008) How lipid flippases can modulate membrane structure. *Biochim Biophys Acta* 1778:1591–1600.
39. Lipowsky R (2013) Spontaneous tubulation of membranes and vesicles reveals membrane tension generated by spontaneous curvature. *Faraday Discuss* 161:305–331, and discussion (2013) 161:419–459.
40. Lenz P, Joanny JF, Jülicher F, Prost J (2003) Membranes with rotating motors. *Phys Rev Lett* 91:108104.
41. Uchida N, Golestanian R (2010) Synchronization and collective dynamics in a carpet of microfluidic rotors. *Phys Rev Lett* 104:178103.
42. Goto Y, Tanaka H (2015) Purely hydrodynamic ordering of rotating disks at a finite Reynolds number. *Nat Commun* 6:5994.
43. Yeo K, Lushi E, Vlahovska PM (2015) Collective dynamics in a binary mixture of hydrodynamically coupled microrotors. *Phys Rev Lett* 114:188301.
44. Aragones JL, Steimel JP, Alexander-Katz A (2016) Elasticity-induced force reversal between active spinning particles in dense passive media. *Nat Commun* 7:11325.
45. van Zuiden BC, Paulose J, Irvine WTM, Bartolo D, Vitelli V (2016) Spatiotemporal order and emergent edge currents in active spinner materials. *Proc Natl Acad Sci USA* 113:12919–12924.
46. Espinosa G, López-Montero I, Monroy F, Langevin D (2011) Shear rheology of lipid monolayers and insights on membrane fluidity. *Proc Natl Acad Sci USA* 108:6008–6013.
47. Matthies D, et al. (2011) Cell-free expression and assembly of ATP synthase. *J Mol Biol* 413:593–603.
48. Spetzler D, et al. (2006) Microsecond time scale rotation measurements of single F1-ATPase molecules. *Biochemistry* 45:3117–3124.
49. Ishmukhametov R, Hornung T, Spetzler D, Frasch WD (2010) Direct observation of stepped proteolipid ring rotation in *E. coli* F0F1-ATP synthase. *EMBO J* 29:3911–3923.
50. Choi SQ, Steltenkamp S, Zasadzinski JA, Squires TM (2011) Active microrheology and simultaneous visualization of sheared phospholipid monolayers. *Nat Commun* 2:312.
51. Rouser G, Fkeischer S, Yamamoto A (1970) Two dimensional then layer chromatographic separation of polar lipids and determination of phospholipids by phosphorus analysis of spots. *Lipids* 5:494–496.
52. Towbin H, Staehelin T, Gordon J (1979) Electrophoretic transfer of proteins from polyacrylamide gels to nitrocellulose sheets: Procedure and some applications. *Proc Natl Acad Sci USA* 76:4350–4354.
53. Schneider CA, Rasband WS, Eliceiri KW (2012) NIH Image to ImageJ: 25 years of image analysis. *Nat Methods* 9:671–675.
54. Johnson LV, Walsh ML, Chen LB (1980) Localization of mitochondria in living cells with rhodamine-123. *Proc Natl Acad Sci USA* 77:990–994.
55. Usenik P, Vrtovec T, Pernuš F, Likar B (2011) Automated tracking and analysis of phospholipid vesicle contours in phase contrast microscopy images. *Med Biol Eng Comput* 49:957–966.
56. Gov N (2004) Membrane undulations driven by force fluctuations of active proteins. *Phys Rev Lett* 93:268104.
57. Manneville JB, Bassereau P, Levy D, Prost J (1999) Activity of transmembrane proteins induces magnification of shape fluctuations of lipid membranes. *Phys Rev Lett* 82:4356–4359.

Almendro-Vedia et al.